**ENCLOSURE 2**

**CNRO-2003-00033**

**ENGINEERING REPORT M-EP-2003-002, REV. 1**

# FRACTURE MECHANICS ANALYSIS FOR THE ASSESSMENT OF THE POTENTIAL FOR PRIMARY WATER STRESS CORROSION CRACK (PWSCC) GROWTH IN THE UNINSPECTED REGIONS OF THE CONTROL ELEMENT DRIVE MECHANISM (CEDM) NOZZLES AT ARKANSAS NUCLEAR ONE UNIT 2

Entergy

**ENTERGY NUCLEAR SOUTH**
**Engineering Report Coversheet**

**Fracture Mechanics Analysis for the Assessment of the Potential for Primary Water Stress Corrosion Crack (PWSCC) Growth in the Un-Inspected Regions of the Control Element Drive Mechanism (CEDM) Nozzles at Arkansas Nuclear One Unit 2**

**Engineering Report Type:**

New Revision X Deleted ☐ Superceded ☐

**Applicable Site(s)**

ANO X Echelon X GGNS ☐ RBS ☐ WF3

**Report Origin:** X ENS ☐ Vendor **Safety-Related:** X Yes ☐ No

Vendor Document No. _____

| | | | Comments: | Attached: |
|---|---|---|---|---|
| Prepared by: | J. S. Bishmadesan<br>Responsible Engineer | Date: 8/26/2003 | ☐ Yes<br>☐ No | ☐ Yes<br>☐ No |
| Verified/ Reviewed by: | Brian C. Gray<br>Design Verifier/Reviewer | Date: 8/26/03 | ☑ Yes<br>☐ No | ☐ Yes<br>☑ No |
| Approved by: | R. S. [illegible]<br>Responsible Supervisor or Responsible Central Engineering Manager (for multiple site reports only) | Date: 8/26/03 | ☐ Yes<br>☑ No | ☐ Yes<br>☐ No |

Engineering Report No. E-M-EP-2003-002 Rev. 01
Page 2 of 62

## RECOMMENDATION FOR APPROVAL FORM

| | | | Comments: | Attached: |
|---|---|---|---|---|
| Prepared by: J. S. Bohmaleson<br>William Simo 8/26/03 Responsible Engineer | Date: 8/27/2003 | | ☐ Yes<br>☐ No | ☐ Yes<br>☐ No |
| Concurrence: Kirk Nuckel<br>Responsible Engineering Manager, ANO | Date: 8/26/03 | | ☐ Yes<br>☒ No | ☐ Yes<br>☐ No |
| Concurrence: **Not Applicable**<br>Responsible Engineering Manager, GGNS | Date: | | ☐ Yes<br>☐ No | ☐ Yes<br>☐ No |
| Concurrence: **Not Applicable**<br>Responsible Engineering Manager, RBS | Date: | | ☐ Yes<br>☐ No | ☐ Yes<br>☐ No |
| Concurrence: **Not Applicable**<br>Responsible Engineering Manager, WF3 | Date: | | ☐ Yes<br>☐ No | ☐ Yes<br>☐ No |

## Table of Contents


| Section | Title | Page Number |
|---|---|---|
| | List of Tables | 3 |
| | List of Figures | 4 |
| | List of Appendices | 6 |
| 1.0 | Introduction | 7 |
| 2.0 | Stress Analysis | 11 |
| 3.0 | Analytical Basis for Fracture Mechanics and Crack Growth Models | 33 |
| 4.0 | Method of Analysis | 38 |
| 5.0 | Discussion and Results | 43 |
| 6.0 | Conclusions | 60 |
| 7.0 | References | 61 |


## List of Tables


| Table Number | Title | Page Number |
|---|---|---|
| 1 | Nodal Stress data for 0° Nozzle. | 17 |
| 2 | Nodal Stress data for the 8.8° nozzle at the downhill location. | 18 |
| 3 | Nodal Stress data for the 8.8° nozzle at 22.5° rotated from the downhill location. | 19 |
| 4 | Nodal Stress data for the 8.8° nozzle at 45° rotated from the downhill location. | 20 |
| 5 | Nodal Stress data for the 8.8° nozzle at 67.5° rotated from the downhill location. | 21 |
| 6 | Nodal Stress data for the 8.8° nozzle at the Mid-Plane location. | 22 |
| 7 | Nodal Stress data for the 8.8° nozzle at the uphill location. | 23 |
| 8 | Nodal Stress data for the 28.8° nozzle at the downhill location. | 24 |

## List of Tables (continued)


| Table Number | Title | Page Number |
|---|---|---|
| 9 | Nodal Stress data for the 28.8° nozzle at 22.5° rotated from the downhill location. | 25 |
| 10 | Nodal Stress data for the 28.8° nozzle at the Mid-Plane location. | 26 |
| 11 | Nodal Stress data for the 28.8° nozzle at the uphill location. | 27 |
| 12 | Nodal Stress data for the 49.6° nozzle at the downhill location. | 28 |
| 13 | Nodal Stress data for the 49.6° nozzle at 22.5° rotated from the downhill location. | 29 |
| 14 | Nodal Stress data for the 49.6° nozzle at 45° rotated from the downhill location. | 30 |
| 15 | Nodal Stress data for the 49.6° nozzle at the Mid-Plane location. | 31 |
| 16 | Nodal Stress data for the 49.6° nozzle at the uphill location. | 32 |
| 17 | Comparison of Fracture Mechanics Models | 48 |
| 18 | Results for compression zone | 49 |
| 19 | ANO-2 As-Built Analyses Results Summary | 51 |
| 20 | Results from Additional Analysis | 56 |
| 21 | Boundaries for Augmented Inspection | 57 |


## List of Figures


| Figure Number | Title | Page Number |
|---|---|---|
| 1 | Details of guide-cone connection to CEDM [2]. Detail extracted from Drawing M-2001-C2-107 [2 | 8 |
| 2 | Sketch of a typical inspection probe sled [3a]. | 9 |
| 3 | Estimated as-built nozzle configuration based on evaluation of the UT and design data. | 12 |
| 4 | Hoop Stress contours for the 0° nozzle. | 14 |
| 5 | Hoop Stress contours for the 8.8° nozzle. | 14 |
| 6 | Hoop Stress contours for the 28.8° nozzle. | 15 |
| 7 | Hoop Stress contours for the 49.6° nozzle. | 15 |
| 8 | Plot showing hoop stress distribution along tube axis for the 0° nozzle. | 17 |
| 9 | Plot showing hoop stress distribution along tube axis for the 8.8° nozzle at the downhill location. | 18 |
| 10 | Plot showing hoop stress distribution along tube axis for the 8.8° nozzle at 22.5° rotated from the downhill location. | 19 |
| 11 | Plot showing hoop stress distribution along tube axis for the 8.8° nozzle at 45° rotated from the downhill location. | 20 |

## List of Figures (Continued)


| Figure Number | Title | Page Number |
|---|---|---|
| 12 | Plot showing hoop stress distribution along tube axis for the 8.8° nozzle at 67.5° rotated from the downhill location. | 21 |
| 13 | Plot showing hoop stress distribution along tube axis for the 8.8° nozzle at the Mid-Plane location. | 22 |
| 14 | Plot showing hoop stress distribution along tube axis for the 8.8° nozzle at the uphill location. | 23 |
| 15 | Plot showing hoop stress distribution along tube axis for the 28.8° nozzle at the downhill location. | 24 |
| 16 | Plot showing hoop stress distribution along tube axis for the 28.8° nozzle at 22.5° rotated from the downhill location.. | 25 |
| 17 | Plot showing hoop stress distribution along tube axis for the 28.8° nozzle at the Mid-Plane location. | 26 |
| 18 | Plot showing hoop stress distribution along tube axis for the 8.8° nozzle at the uphill location. | 27 |
| 19 | Plot showing hoop stress distribution along tube axis for the 49.6° nozzle at the downhill location. | 28 |
| 20 | Plot showing hoop stress distribution along tube axis for the 49.6° nozzle at 22.5° rotated from the downhill location. | 29 |
| 21 | Plot showing hoop stress distribution along tube axis for the 49.6° nozzle at 45° rotated from the downhill location. | 30 |
| 22 | Plot showing hoop stress distribution along tube axis for the 49.6° nozzle at the Mid-Plane location. | 31 |
| 23 | Plot showing hoop stress distribution along tube axis for the 49.6° nozzle at the uphill location. | 32 |
| 24 | SICF shown as a function of normalized crack depth for the "a-tip" and the "c-tip" | 34 |
| 25 | Curve fit equations for the "extension and bending" components in Reference 8. | 37 |
| 26 | Plots showing effect of nodal data selection on the accuracy of polynomial regression fit, | 41 |
| 27 | Comparison of SICF for the edge crack configurations with the membrane SICF for current model. | 46 |
| 28 | Comparison of SIF for the current model and conventional model. | 47 |
| 29 | SIF comparison between current model and conventional model. | 48 |
| 30 | Crack growth and SIF for 0° nozzle – OD surface crack. | 52 |

## List of Figures (Continued)


| Figure Number | Title | Page Number |
|---|---|---|
| 31 | Crack growth and SIF for 0° nozzle – Through-wall axial crack. | 53 |
| 32 | Crack growth and SIF for 8.8° nozzle – OD surface crack. | 53 |
| 33 | Crack growth and SIF for 8.8° nozzle – Through-wall axial crack. | 54 |
| 34 | Crack growth and SIF for 28.8° nozzle – OD surface crack. | 54 |
| 35 | Crack growth and SIF for 28.8° nozzle – Through-wall axial crack. | 55 |
| 36 | 0° Nozzle crack growth at a lowered reference line at 1.25 inches above nozzle bottom. | 58 |
| 37 | 8.8° Nozzle crack growth at blind zone elevation of 1.544 inches above nozzle bottom at an azimuth of 67.5°. | 58 |
| 38 | 28.8° Nozzle crack growth at blind zone elevation of 1.544 inches above nozzle bottom at an azimuth of 22.5°. | 59 |
| 39 | 49.6° Nozzle crack growth at blind zone elevation of 1.544 inches above nozzle bottom at an azimuth of 45°. | 60 |


## List of Appendices


| Appendix Number | Content of Appendix | Number of Attachments In Appendix |
|---|---|---|
| A | Design, UT probe characterization, UT analysis results, and evaluation for as-built configuration | 6 |
| B | Mathcad worksheets annotated to describe the three models | 3 |
| C | Mathcad worksheets for ANO-2 Analyses | 48[1] |
| D | Verification and Comparisons (Mathcad worksheets) | 4 |


1) Attachment number 32 is intentionally blank, but is included to keep the sequence in order.

**Note:- This document {revision 1} was revised to:**

**1) Make it ANO-2 specific.**

**2) Revise finite element models and re-analyze residual stresses.**

**3) Change the surface crack fracture mechanics models.**

**4) Define augmented inspection regions.**

## 1.0 Introduction

The US Nuclear Regulatory Commission (NRC) issued Order EA-03-009 [1], which modified licenses, requiring inspection of all Control Element Drive Mechanism (CEDM), In-Core Instrumentation (ICI), and vent penetration nozzles in the reactor vessel head. Paragraph IV.C.1.b of the Order requires the inspection to cover a region from the bottom of the nozzle to two (2.0) inches above the J-groove weld. In the Combustion Engineering (CE) design the CEDM nozzles have a guide-cone attached to the bottom of each CEDM. Figure 1 [2] provides a drawing showing the attachment detail and a sketch showing the typical CEDM arrangement in the reactor vessel head. The attachment is a threaded connection with a securing set-screw between the guide-cone and the CEDM nozzle. The CEDM nozzle is internally threaded and the guide-cone has external threads. Thus, the CEDM nozzles in the region of attachment, including the chamfered region, become inaccessible for Ultrasonic Testing (UT) to interrogate the nozzle base material. The design of the UT probes result in a region above the chamfer (0.200 inch [reference 3a &3b]) that cannot be inspected. Therefore, the region of the CEDM base metal that <u>can</u> be inspected begins at about 1.544 inches above the bottom of the CEDM nozzle and extends to two (2.0) inches above the J-groove weld. The unexamined length (here after called the blind zone) constitutes the threaded region, the chamfer region, and the UT dead zone (1.250 + 0.094 + 0.200). The terms used in this report are defined as follows:

- Freespan = (bottom of weld – blind zone); this area below the weld is accessible for volumetric examination.
- Propagation Length = (bottom of weld –top of crack tip); area available for crack growth.

  *Note:- for an outside diameter (OD) surface crack, this length is always less than the freespan; for through-wall it is equal to the freespan; and, for an inside diameter (ID) surface crack, the criterion is the propagation length and a through-wall penetration condition.*
- Augmented Inspection Area: The axial and circumferential extent of the CEDM below the blind zone subject to an OD surface examination to ensure sufficient region for crack growth in one (1) cycle of operation without compromising the weld. This region may include weld material when the weld extends into the blind zone.

The nozzle as-built dimensions were determined by a detailed review of applicable design drawings and UT data from the previous inspection, which are provided as an attachment in Appendix A. The results of this assessment was used to develop the finite element model which obtains the prevailing stress distribution (Residual+Operating) used in the deterministic fracture mechanics analyses. The deterministic fracture mechanics analyses, in turn, assess the potential for primary water stress corrosion cracking (PWSCC) in the blind zone of the nozzles. This aspect is discussed in more detail in Section 2.

In order to exclude the blind zone from the inspection campaign, a relaxation of the Order is required pursuant to the requirements prescribed in Section IV.F and footnote 2 of the Order [1].

The purpose of this engineering report is to:

1. Determine if sufficient area between the blind zone and the weld exists to facilitate one (1) cycle of axial crack growth without the crack reaching the weld, and
2. For nozzles not meeting 1 above, determine how much of the blind zone combined with the available freespan is required to facilitate 1 cycle of crack growth without the crack reaching the weld. This area is subject to augmented surface examination.

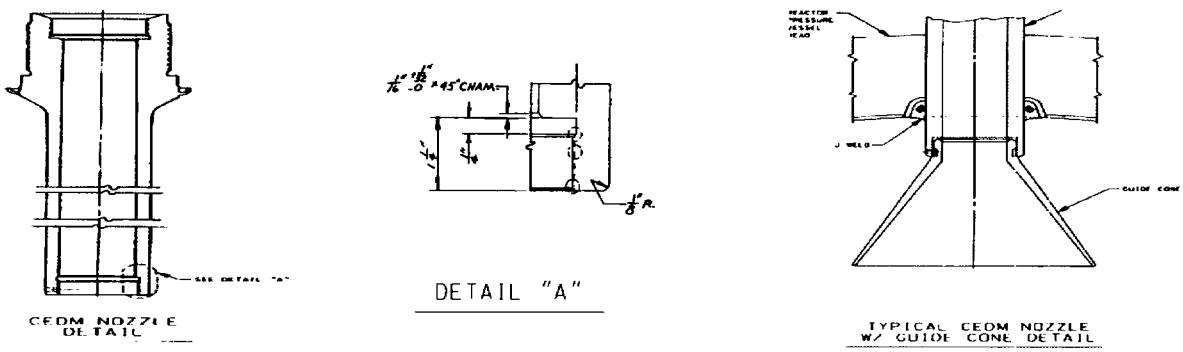


a b c

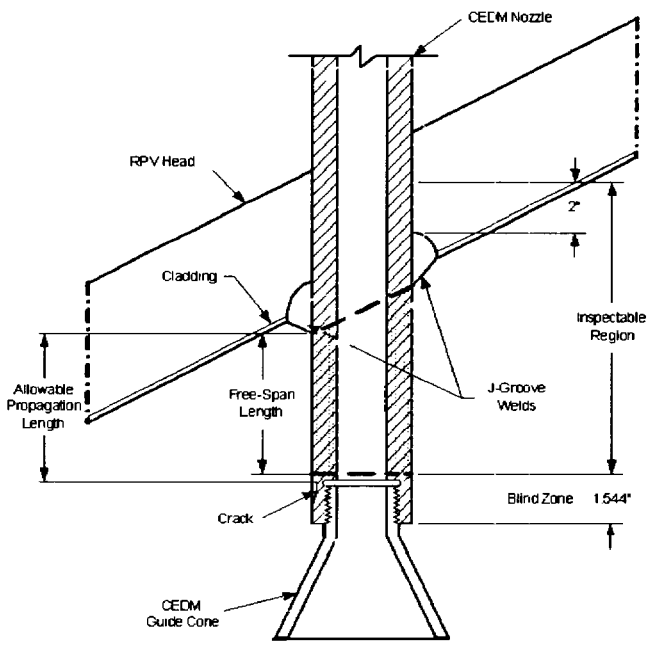


d

**Figure 1:**

*Details of guide cone connection to CEDM[2]. A sketch of a typical CEDM connection showing regions of interest is provided.*

a) *CEDM nozzle tube.*

b) *Details of the chamfer in the machined recess of the threaded region. Provides dimensions for the threaded and chamfer regions.*

c) *Details of guide-cone connection to CEDM [2].*

d) *Sketch of a typical CEDM penetration showing the region of interest.*

*Detail extracted from Drawing M-2001-C2-23 (ANO-2) [2]. The threaded region in the CEDM is 1.344 inches (Threads plus Recess plus chamfer).*

The detail of the guide-cone-to-CEDM connection shows that the threaded + chamfer region is 1.344 inches in height. The UT dead band, determined to be 0.200 inch above the top of the threaded plus chamfer region in the CEDM, is based on a typical inspection probe sled design [3b] (shown in Figure 2).

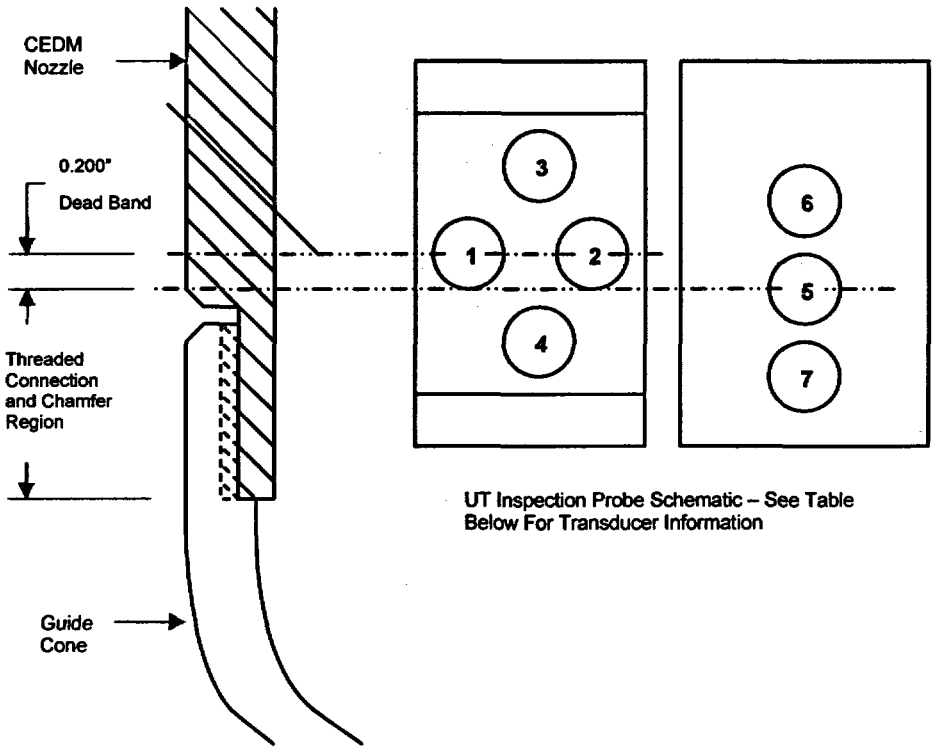


| Position | Mode | Diameter | Description |
|---|---|---|---|
| 1 | Transmit | 0.25" | Circumferential Scan Using TOFD |
| 2 | Receive | 0.25" | Circumferential Scan Using TOFD |
| 3 | Transmit | 0.25" | Axial Scan Using TOFD |
| 4 | Receive | 0.25" | Axial Scan Using TOFD |
| 5 | Transmit<br>Receive | 0.25" | Standard Zero Degree Scan |
| 6 | LFEC | NA | Low Frequency Eddy Current Probe |
| 7 | EC | NA | Standard Driver/Pickup Eddy Current Probe |

**Figure 2:** *Sketch of a typical inspection probe sled [3a]. The UT dead band is shown with respect to the thread + chamfer region*

Based on the probe design and the geometry of the nozzle at the threaded connection, the explanation provided in Reference 3b shows the UT dead band to

extend 0.200 inch above the chamfer region immediately above the threads. Therefore, to account for the thread region, chamfer and the UT dead band, the blind zone height is determined to be 1.544 inch (1.250" + 0.094" + 0.2") above the bottom of the nozzle.

The analysis used to determine the impact of not examining the blind zone independently evaluates a part through-wall axial crack initiated from the ID, a part through-wall axial crack initiated from the OD, and a through-wall axial crack.

*Part Through-Wall Cracks*

The initial crack depth obtained from Reference 4 is 0.04627 inch deep for an ID axial crack and 0.07932 inch deep for an OD axial crack. The crack length is based on the detected length of 4 mm (0.157 inch) from Reference 4. In the deterministic fracture mechanics analyses, the part through-wall crack lengths are doubled to 0.32 inch and the crack center is located at the top of the blind zone. Thus, the crack spans both the blind zone and the inspectable region. The postulated crack sizes and depths are two times the detectable limits with one-half (0.16 inch) of the flaw length being located in the examinable area. This provides for a conservative evaluation because:

A) By extending the postulated crack 0.16 inch into the inspectable region, it places the crack tip closer to the weld where the hoop stresses are higher; and

B) it assumes that 0.16 inches of the inspectable region is already cracked, reducing the remaining area for crack propagation.

*Through-Wall Crack*

In addition to evaluating the part through-wall cracks, this evaluation also conservatively evaluates a through-wall axial crack. The through-wall axial crack is postulated to exist from the top of the blind zone down to a point where the hoop stress is $\leq$ 10 ksi. This is a very conservative assumption, because for a crack to initiate on the surface and propagate through-wall while being totally contained within the blind zone would result in an unrealistic aspect ratio. As can be concluded from the following analysis, the length of a part through-wall crack would propagate into the inspectable region long before its depth reaches a through-wall condition. However, evaluation of the through-wall crack provides completeness to this assessment and ensures all plausible crack propagation modes are considered. Like the part through-wall crack, the hoop stresses at the top of the blind zone were used as the initial stress with adjustments to account for the increased stresses as the crack approaches the weld.

The analyses include a finite element stress analysis of the CEDM nozzles and a fracture mechanics-based crack growth analysis for PWSCC. These analyses are

performed for four nozzles (the nozzles were chosen at four head angles 0°, 8.8°, 28.8°, and 49.6°) in the reactor vessel head to account for the varied geometry of the nozzle penetration. In this manner the analysis provides a bounding evaluation for all nozzles in the reactor vessel head. The sections that follow contain a description of the analyses, the results, and conclusions supported by the analyses.

## 2.0 Stress Analysis

Finite element-based stress analyses for the ANO-2 CEDM penetrations, using the highest tensile yield strength for each group of nozzles, were performed using the best-estimate geometries based on previous UT and design information. The UT data obtained at the previous refueling outage were reviewed to determine the locations of the top and bottom of the J-weld at two azimuthal locations, downhill (0°) and the uphill (180°). The UT data obtained from this analysis is presented in Appendix A. This UT data were compared to the design information obtained from design drawings using an Excel spreadsheet to estimate the as-built condition. The spreadsheet used in this analysis is presented in Appendix A. This evaluation showed the following:

1) The central CEDM nozzles (0° and 8.8°) have weld sizes that are similar in size to the design drawings. However, this analysis also showed that the nozzle length below the ID clad surface to be 2.08 inches (shorter by 0.4 inch) compared to the design length of 2.48 inches.
2) The downhill side fillet welds on the peripheral CEDM nozzles (28.8° and 49.6°) have a longer leg than estimated from the design information. A fillet weld radius of 3/8 inch instead of the specified 3/16 inch provided the fillet weld leg length that matched the UT data. This evidence was also observed in another CE fabricated reactor vessel head. The fillet weld on the uphill side matched the information on the design drawing. Thus, only the downhill side fillet weld leg was extended for the model. The weld length on the uphill side matched the design information.

The evaluation to estimate the as-built dimensions of the CEDM configuration, taking into consideration the UT data and design information, consisted of the following steps:

1) The blind zone elevation of 1.544 inches from the nozzle bottom was taken to exist for all CEDM nozzles.
2) The design lengths for freespan at both the downhill and uphill locations were established (design length from weld bottom – blind zone).
3) These values were compared to the measurements obtained from the UT data analysis. The differences were recorded.
4) The design length to the top of the J-weld was compared to the measured length from the UT data for both the downhill and uphill locations and the differences recorded.

5) The weld lengths from design drawings were compared to the as measured data from the UT results. This was done for both the downhill and uphill locations. The differences were recorded.

6) The differences were evaluated to assess the variation between the design and as-measured data. This comparison showed that the differences for the central nozzles (8.8°) were consistent but the differences at the uphill location was 0.53 inch and a downhill freespan location was about 0.33 inch. This variation could be reconciled if the nozzle was about 0.4 inch shorter than the design insertion length. Therefore, the design insertion length was reduced by 0.4 inch to minimize the variation between the as-measured and design data. The higher hillside angle nozzles (28.8° and 49.6°) showed the variation to be more on the downhill side indicating a longer fillet weld leg length. This variation was minimized when the fillet weld radius was changed to 3/8 inch instead of the design specified value of 3/16 inch. Similar findings have been observed for another reactor vessel head fabricated by CE. Therefore, the increased fillet weld radius reasonably explains the larger fillet weld leg length observed in the UT data. For these nozzles the fillet weld leg length was increased. Figure 3 presents the sketches for the higher hillside angle nozzles (28.8° and 49.6°). This geometry was used to develop the estimated as-built finite element model. For the central nozzle group (0° and 8.8°), the nozzle insertion length was shortened by 0.4 inch to 2.08 inches. Since the weld lengths measured from the UT data matched the design data, the finite element model was developed using the shorter length but using the as-designed fillet weld dimensions.

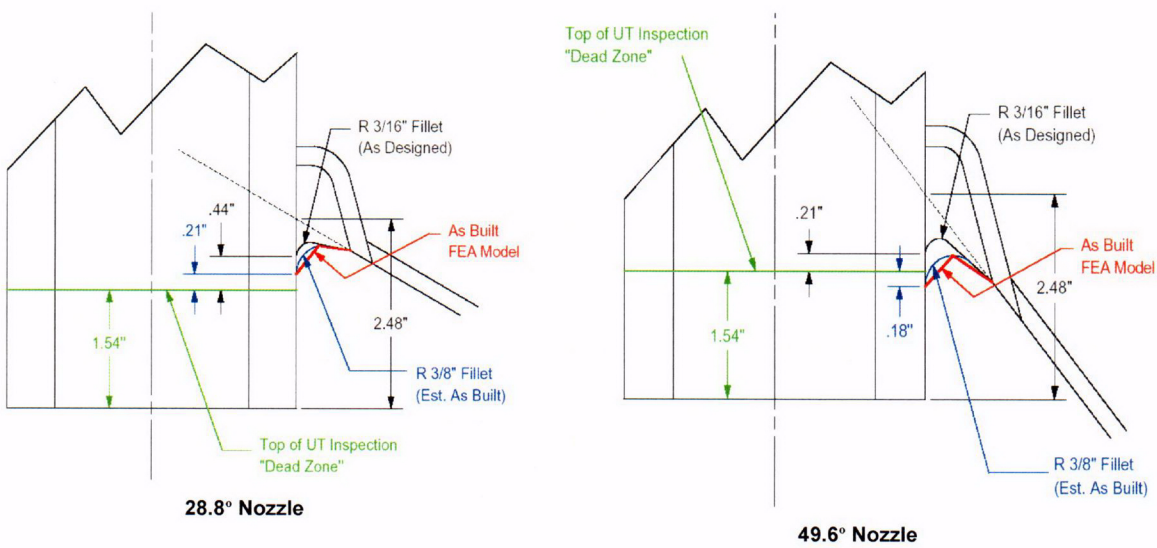


**Figure 3:** *Estimated as-built nozzle configuration based on evaluation of the UT and design data. For the 49.6° nozzle, the bottom of the fillet weld extends 0.18 inch below the blind zone. For the 28.8° nozzle, the freespan length is reduced to 0.21 inch from the as-designed condition of 0.44 inch.*

C01

The finite element modeling for obtaining the necessary stress (residual+operating) distribution for use in fracture mechanics analysis followed the process and methodology described in Reference 5a. The modeling steps were as follows:

1) The finite element mesh consisted of 3-dimensional solid (brick) elements. Four elements were used to model the tube wall and similar refinement was carried to the attaching J-weld.

2) The CEDM tube material was modeled with a monotonic stress strain curve. The highest yield strength from the nozzle material bounded by the nozzle group was used. This yield strength was referenced to the room temperature yield strength of the stress-strain curve described in Reference 5a. The temperature dependent stress strain curves were obtained by indexing the temperature dependent drop of yield strength.

3) The weld material was modeled as elastic-perfectly plastic for the weld simulation. This approximation is considered reasonable since most of the plastic strain in the weld metal occurs at high temperatures where metals do not work-harden significantly (Reference 5c). The temperature in the weld is always high during the welding process and once the weld begins to cool, the temperatures in the weld at which strain hardening would persist are of limited duration (Reference 5c). This was borne out by the comparison between the analysis based residual stress distribution and that obtained from experiments (Reference 5d).

4) The weld is simulated by two passes based on studies presented in Reference 5a.

5) After completing the weld, a simulated hydro-test load step is applied to the model. The hydro-test step followed the fabrication practice.

6) The model is then subjected to a normal operating schedule of normal heat up to steady state conditions at operating pressure. The residual plus operating stresses, once steady state has been achieved, are obtained for further analysis. The nodal stresses of interest are stored in an output file. These stresses are then transferred to an Excel spreadsheet for use in fracture mechanics analysis.

The stress contours for the four nozzle groups obtained from the finite element analysis are presented in Figures 4 through 7. The stress contour color scheme are as follows:

| | |
|---|---|
| *Dark Navy blue* | *from Minimum (Compression) to -10 ksi* |
| *Royal blue* | *from -10 to 0 ksi* |
| *Light blue* | *from 0 to 10 ksi* |
| *Light green* | *from 10 to 20 ksi* |
| *Green* | *from 20 to 30 ksi* |
| *Yellow green* | *from 30 to 40 ksi* |
| *Yellow* | *from 40 to 50 ksi* |
| *Red* | *from 50 to 100 ksi* |

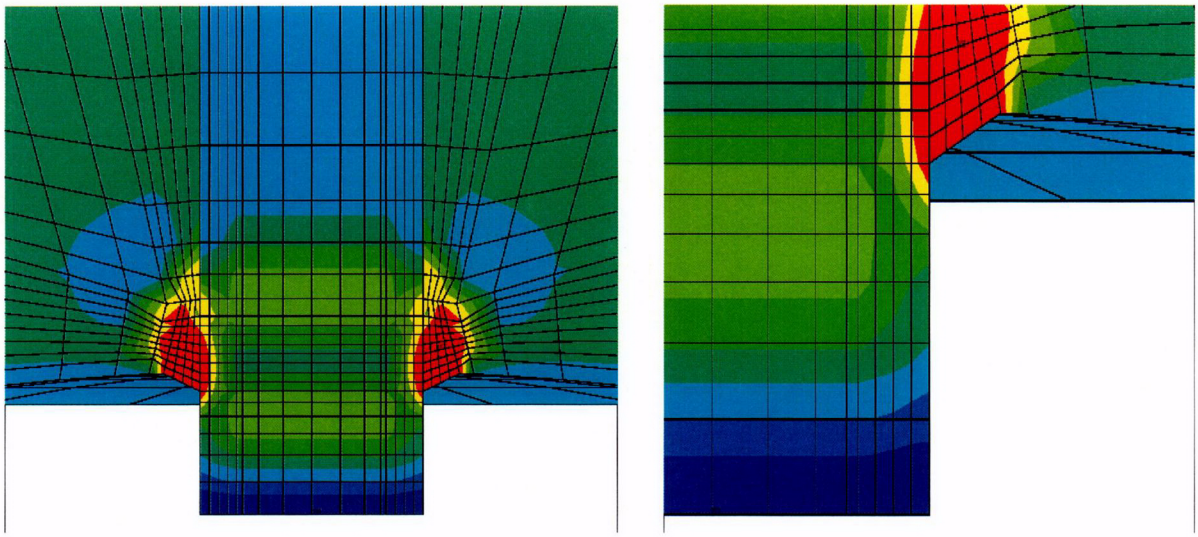

**Full Cross-section** **Zoomed in right weld**

**Figure 4:** *Hoop stress contours for the 0° nozzle. High tensile stresses occur in the weld and adjacent tube material. The bottom of the tube is in compression.*

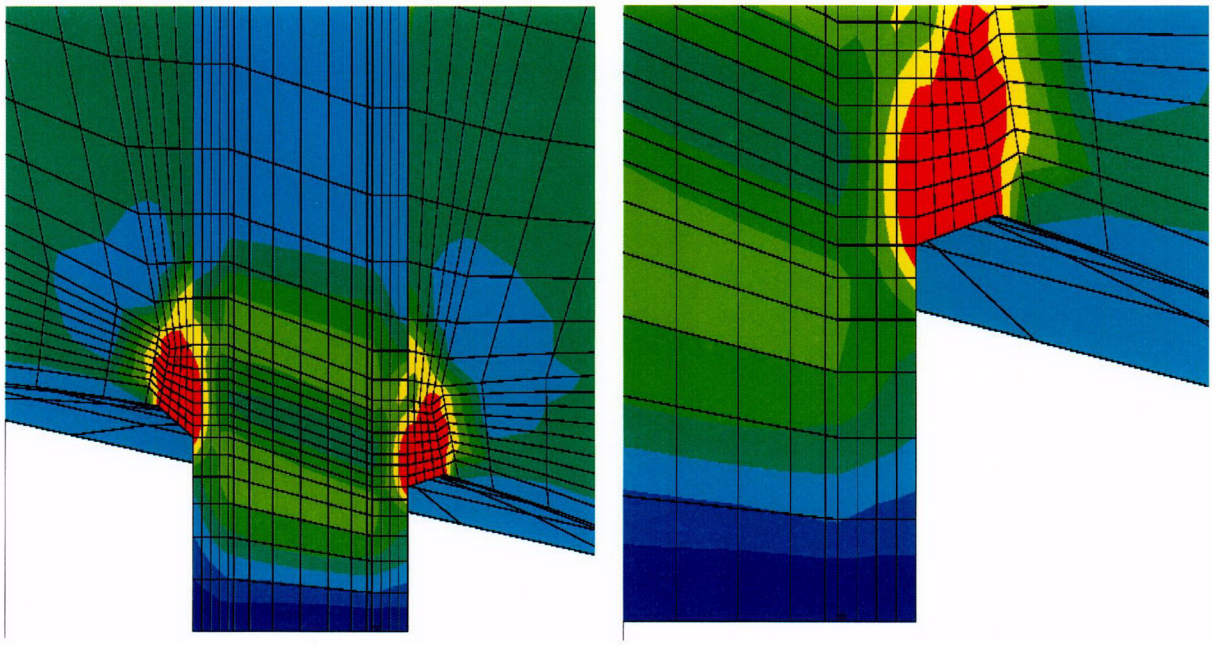

**Full cross-section** **Zoomed in Downhill side**

**Figure 5:** *Hoop stress contours for the 8.8° nozzle. High tensile stresses occur in the weld and adjacent tube material. The bottom of the tube is in compression.*

C02

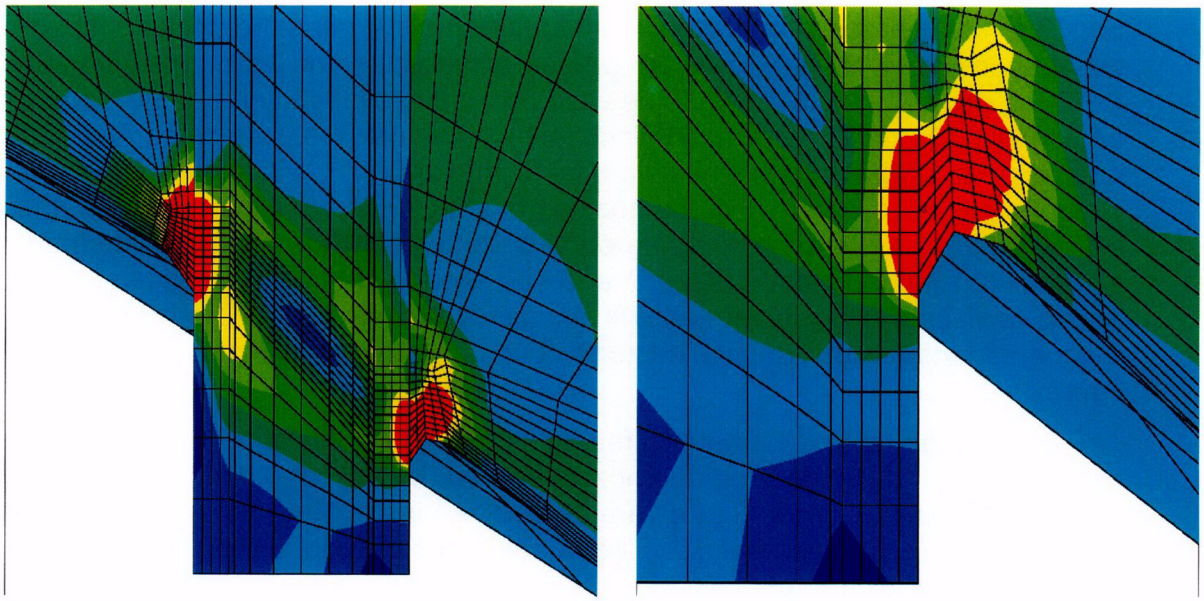

**Full cross-section** **Zoomed in Downhill side**

**Figure 6:** *Hoop stress contours for the 28.8° nozzle. High tensile stresses occur in the weld and adjacent tube material. The bottom of the tube is in compression.*

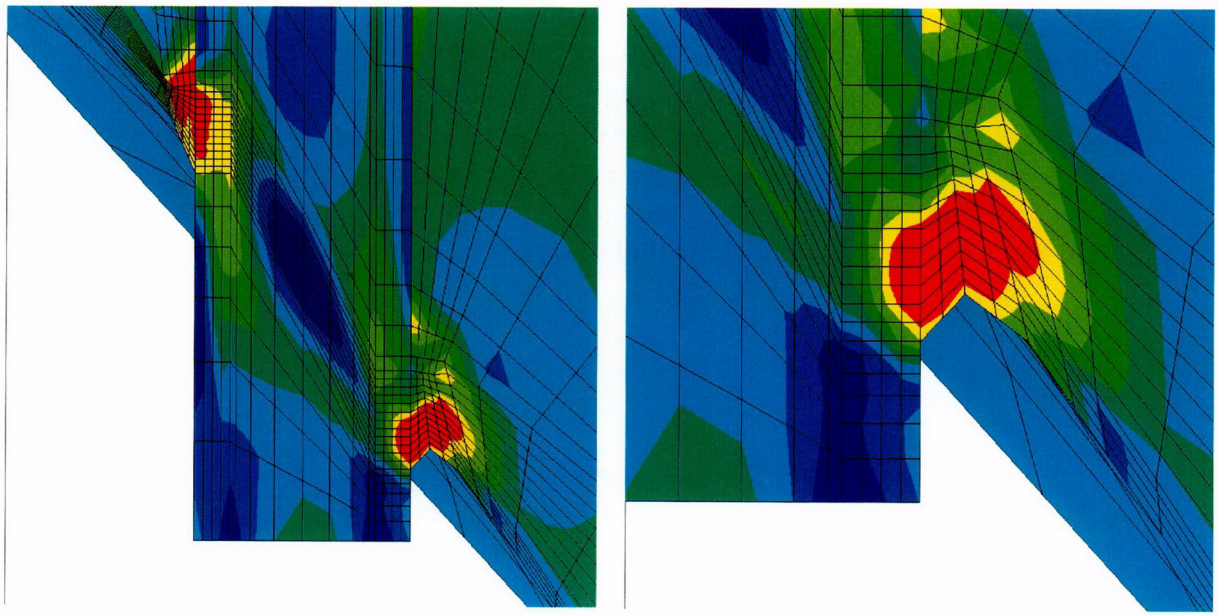

**Full cross-section** **Zoomed in Downhill side**

**Figure 7:** *Hoop stress contours for the 49.6° nozzle. High tensile stresses occur in the weld and adjacent tube material. The bottom of the tube is in compression.*

The nodal stresses for the locations of interest in each of the four nozzle groups were provided by Dominion Engineering Inc. and were tabulated in Reference

5b. The nodal stresses and associated figures representing the OD and ID distributions along the tube axis are presented in tables and associated figures in the following pages. The location of the weld bottom was maintained at the node row ending with "601". The blind zone location is shown on the associated figure. For the nozzle group at 8.8°, additional azimuthal locations (22.5°, 45° and 67.5°) around the circumference are shown. For the nozzle group at 28.8°, an additional azimuthal location (22.5°) around the circumference is shown. For the nozzle group at 49.6°, additional azimuthal locations (22.5° and 45°) around the circumference are shown. These additional locations are shown since they were evaluated for establishing the augmented inspection scope. The zone of compressive stress is also marked in the figure.

From the tables and associated figures, a full visualization of the stress distribution in the nozzle, from the nozzle bottom (located at 0.0 inch) to the top of the J-weld is obtained. These figures are also shown in the Mathcad worksheets provided in the Appendix "C" attachments. The nodal stress distribution, provided by Dominion Engineering, is used to establish the region of interest and the associated stress distribution that will be utilized in the subsequent analyses. In all cases evaluated but one, the bottom end of the nozzle (free end) is observed to be in compression. This is expected since the tube in the vicinity of the weld is in tension (high hoop tension), and the normal decay of stresses along the length of the tube results in compressive stress at the bottom. When the weld bottom extends lower, the compressive zone is shortened, but there remains a zone of compressive stress at the free end. For the 49.6° nozzle at the 90° rotated from the downhill location, the ID stress remains in tension while the OD stress becomes compressive (Figure 22)

In the following pages, the stress data from the Excel spreadsheet provided by Dominion Engineering (Reference 5b) and plots representing the axial distribution at the ID and OD locations are presented for each nozzle group with the specific azimuthal location that is evaluated. The location of the compression zone the blind zone and bottom of the weld are marked by colored reference lines.

| Row | Height | ID | 25% | 50% | 75% | OD |
|---|---|---|---|---|---|---|
| 1 | 0.000 | -25.088 | -27.546 | -27.787 | -25.624 | -23.763 |
| 101 | 0.485 | -0.56305 | -0.53856 | -2.1108 | -4.851 | -6.1565 |
| 201 | 0.874 | 21.515 | 18.635 | 17.122 | 14.843 | 10.089 |
| 301 | 1.186 | 32.751 | 28.494 | 24.136 | 19.645 | 14.45 |
| 401 | 1.436 | 35.667 | 29.598 | 26.166 | 25.589 | 28.417 |
| 501 | 1.635 | 34.244 | 29.574 | 28.286 | 35.408 | 45.379 |
| 601 | 1.796 | 29.45 | 29.814 | 31.385 | 43.337 | 61.713 |
| 701 | 1.932 | 23.674 | 26.502 | 33.261 | 47.609 | 64.65 |
| 801 | 2.068 | 18.928 | 24.564 | 33.968 | 49.071 | 65.876 |
| 901 | 2.204 | 16.541 | 22.854 | 34.789 | 49.525 | 62.795 |
| 1001 | 2.341 | 17.561 | 22.683 | 33.806 | 47.49 | 63.558 |
| 1101 | 2.477 | 22.026 | 23.229 | 32.421 | 44.118 | 58.478 |
| 1201 | 2.613 | 26.382 | 25.611 | 31.17 | 41.606 | 52.552 |
| 1301 | 2.750 | 30.043 | 28.69 | 33.688 | 38.959 | 45.295 |
| 1401 | 2.886 | 33.132 | 31.073 | 37.166 | 43.676 | 36.261 |

**Table 1:** *Nodal stress for 0° nozzle. This nozzle is symmetric about the nozzle axis hence these stresses prevail over the entire circumference. The weld location is shown by the shaded row.*

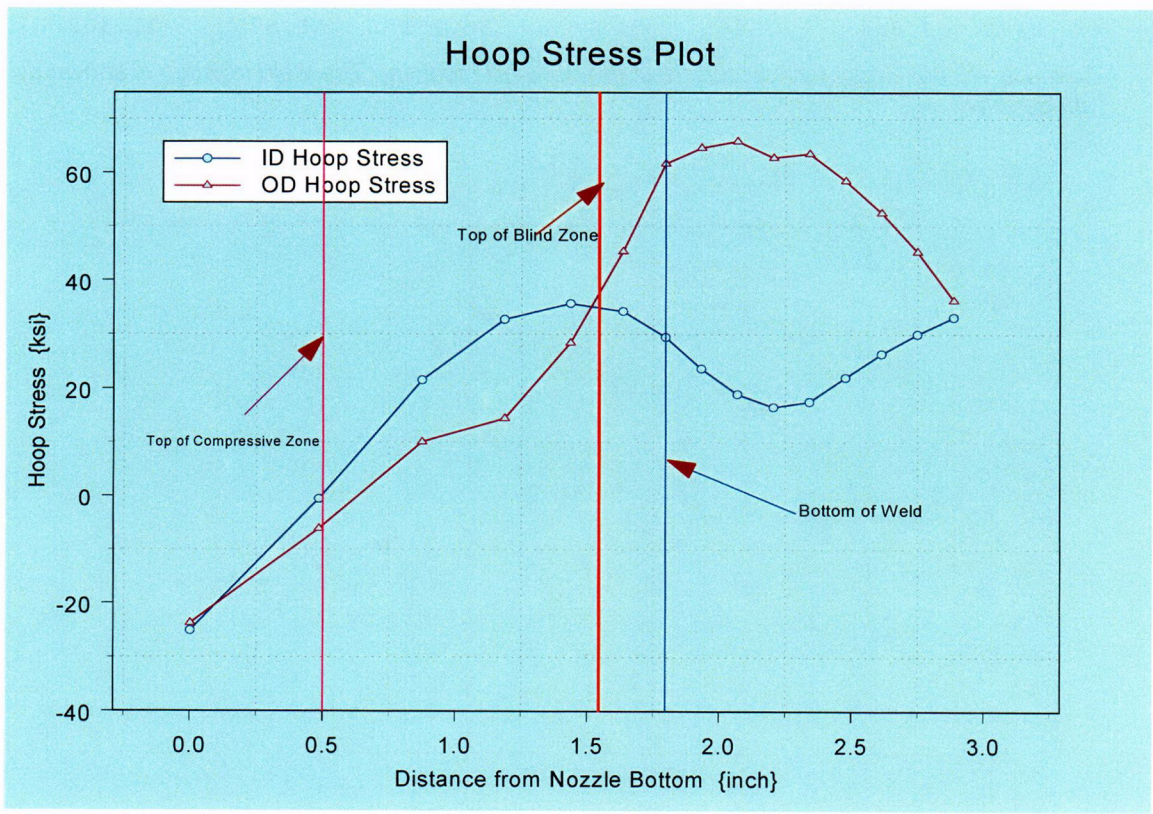


**Figure 8:** *Plot showing hoop stress distribution along tube axis for the 0° nozzle. The top of compressive zone, the top of blind zone, and the bottom of the weld are shown.*

C04

| Row | Height | ID | 25% | 50% | 75% | OD |
|---|---|---|---|---|---|---|
| 1 | 0.000 | -27.404 | -24.356 | -22.209 | -20.407 | -18.978 |
| 101 | 0.483 | 0.63328 | -1.486 | -3.5987 | -4.4402 | -5.2679 |
| 201 | 0.870 | 17.665 | 16.422 | 14.61 | 12.415 | 9.3756 |
| 301 | 1.180 | 29.798 | 26.049 | 22.723 | 18.95 | 14.201 |
| 401 | 1.428 | 33.623 | 27.792 | 24.8 | 24.321 | 26.989 |
| 501 | 1.627 | 32.364 | 28.469 | 27.591 | 34.284 | 45.104 |
| 601 | 1.786 | 27.394 | 28.918 | 31.388 | 43.882 | 63.718 |
| 701 | 1.919 | 21.498 | 25.556 | 33.55 | 48.089 | 66.365 |
| 801 | 2.051 | 16.944 | 23.793 | 34.064 | 49.472 | 67.672 |
| 901 | 2.183 | 14.834 | 22.263 | 34.779 | 49.055 | 63.377 |
| 1001 | 2.315 | 15.852 | 21.898 | 33.764 | 46.61 | 61.537 |
| 1101 | 2.448 | 20.835 | 22.531 | 32.095 | 42.501 | 53.972 |
| 1201 | 2.580 | 25.973 | 25.072 | 30.748 | 39.365 | 47.486 |
| 1301 | 2.712 | 29.955 | 28.372 | 32.593 | 36.879 | 39.934 |
| 1401 | 2.844 | 33.46 | 31.26 | 36.351 | 41.573 | 31.302 |

**Table 2:** *Nodal stress for 8.8° nozzle at the downhill location. The weld location is shown by the shaded row.*

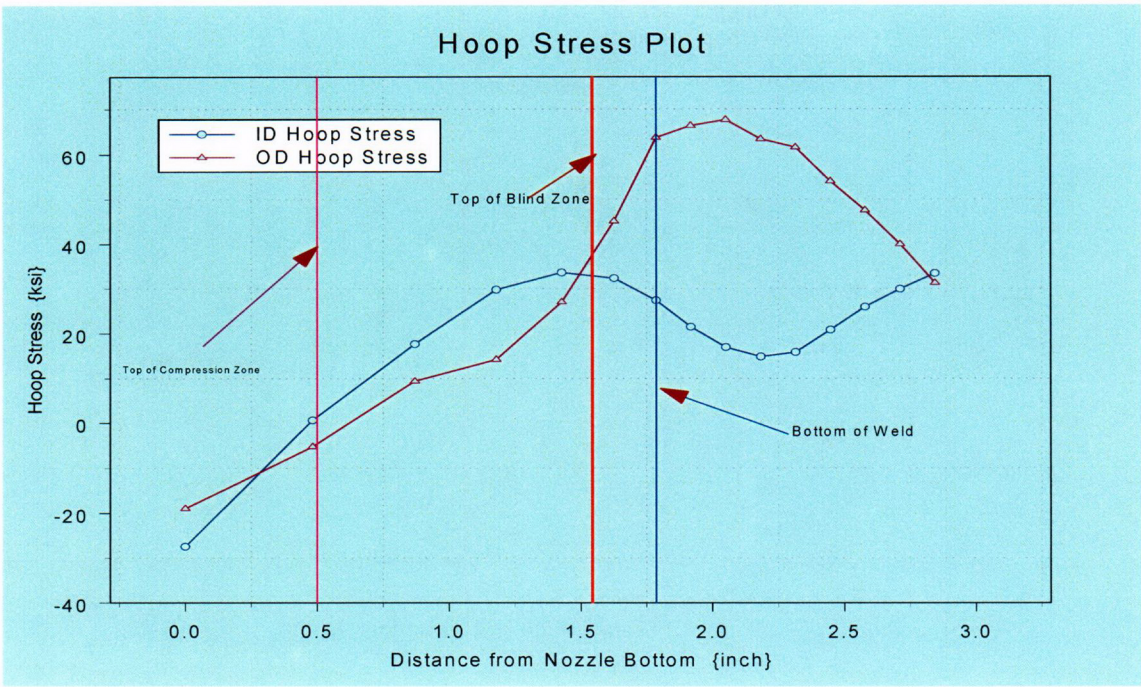


**Figure 9:** *Plot showing hoop stress distribution along tube axis for the 8.8° nozzle at the downhill location. The top of compressive zone, the top of blind zone, and the bottom of the weld are shown.*

C05

| Row | Height | ID | 25% | 50% | 75% | OD |
|---|---|---|---|---|---|---|
| 10001 | 0 | -27.118 | -24.146 | -22.087 | -20.358 | -18.981 |
| 10101 | 0.48843 | 0.64978 | -1.526 | -3.6985 | -4.5989 | -5.4683 |
| 10201 | 0.87972 | 17.955 | 16.435 | 14.447 | 12.118 | 8.9948 |
| 10301 | 1.1932 | 29.829 | 26.102 | 22.672 | 18.714 | 13.833 |
| 10401 | 1.4443 | 33.679 | 27.823 | 24.722 | 24.104 | 26.541 |
| 10501 | 1.6455 | 32.389 | 28.385 | 27.447 | 34.121 | 44.818 |
| 10601 | 1.8067 | 27.386 | 28.803 | 31.156 | 43.603 | 61.245 |
| 10701 | 1.9403 | 21.477 | 25.458 | 33.3 | 47.738 | 65.934 |
| 10801 | 2.074 | 16.919 | 23.701 | 33.846 | 49.217 | 67.244 |
| 10901 | 2.2076 | 14.769 | 22.095 | 34.557 | 48.869 | 62.964 |
| 11001 | 2.3413 | 15.756 | 21.725 | 33.561 | 46.369 | 61.153 |
| 11101 | 2.4749 | 20.717 | 22.317 | 31.908 | 42.308 | 53.889 |
| 11201 | 2.6085 | 25.789 | 24.923 | 30.579 | 39.284 | 47.365 |
| 11301 | 2.7422 | 29.737 | 28.248 | 32.847 | 37.236 | 40.412 |
| 11401 | 2.8758 | 33.001 | 30.843 | 35.887 | 41.552 | 34.5 |

**Table 3:** *Nodal stress for 8.8° nozzle at 22.5° rotated from the downhill location. The weld location is shown by the shaded row.*

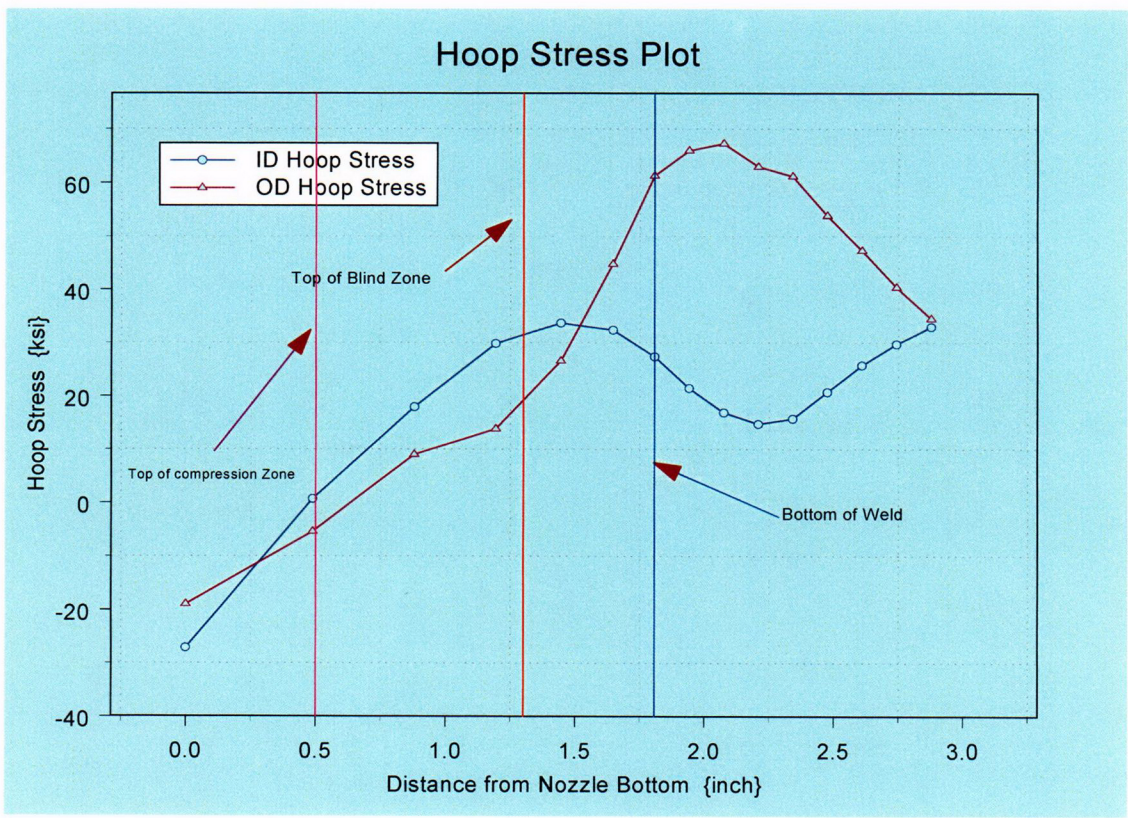


**Figure 10:** *Plot showing hoop stress distribution along tube axis for the 8.8° nozzle at 22.5° rotated from the downhill location. The top of compressive zone, the top of blind zone, and the bottom of the weld are shown.*

C06

| Row | Height | ID | 25% | 50% | 75% | OD |
|---|---|---|---|---|---|---|
| 20001 | 0 | -26.311 | -23.544 | -21.718 | -20.18 | -18.943 |
| 20101 | 0.50592 | -0.3769 | -2.2224 | -3.9683 | -5.0362 | -6.0278 |
| 20201 | 0.91123 | 20.089 | 16.851 | 14.017 | 11.337 | 7.9165 |
| 20301 | 1.2359 | 29.934 | 26.239 | 22.486 | 18.067 | 12.788 |
| 20401 | 1.4961 | 33.829 | 27.906 | 24.526 | 23.554 | 25.421 |
| 20501 | 1.7045 | 32.487 | 28.206 | 27.053 | 33.58 | 44.169 |
| 20601 | 1.8714 | 27.432 | 28.598 | 30.659 | 42.946 | 60.214 |
| 20701 | 2.0063 | 21.433 | 25.168 | 32.645 | 46.971 | 64.949 |
| 20801 | 2.1413 | 16.793 | 23.322 | 33.237 | 48.59 | 66.19 |
| 20901 | 2.2762 | 14.561 | 21.627 | 33.983 | 48.342 | 62.067 |
| 21001 | 2.4111 | 15.505 | 21.303 | 33.027 | 45.936 | 60.887 |
| 21101 | 2.5461 | 20.329 | 21.914 | 31.51 | 42.056 | 54.174 |
| 21201 | 2.681 | 25.223 | 24.532 | 30.274 | 39.283 | 47.704 |
| 21301 | 2.8159 | 29.209 | 27.786 | 32.709 | 37.408 | 41.335 |
| 21401 | 2.9509 | 32.564 | 30.324 | 35.521 | 41.82 | 35.243 |

**Table 4:** *Nodal stress for 8.8° nozzle at 45° rotated from the downhill location. The weld location is shown by the shaded row.*

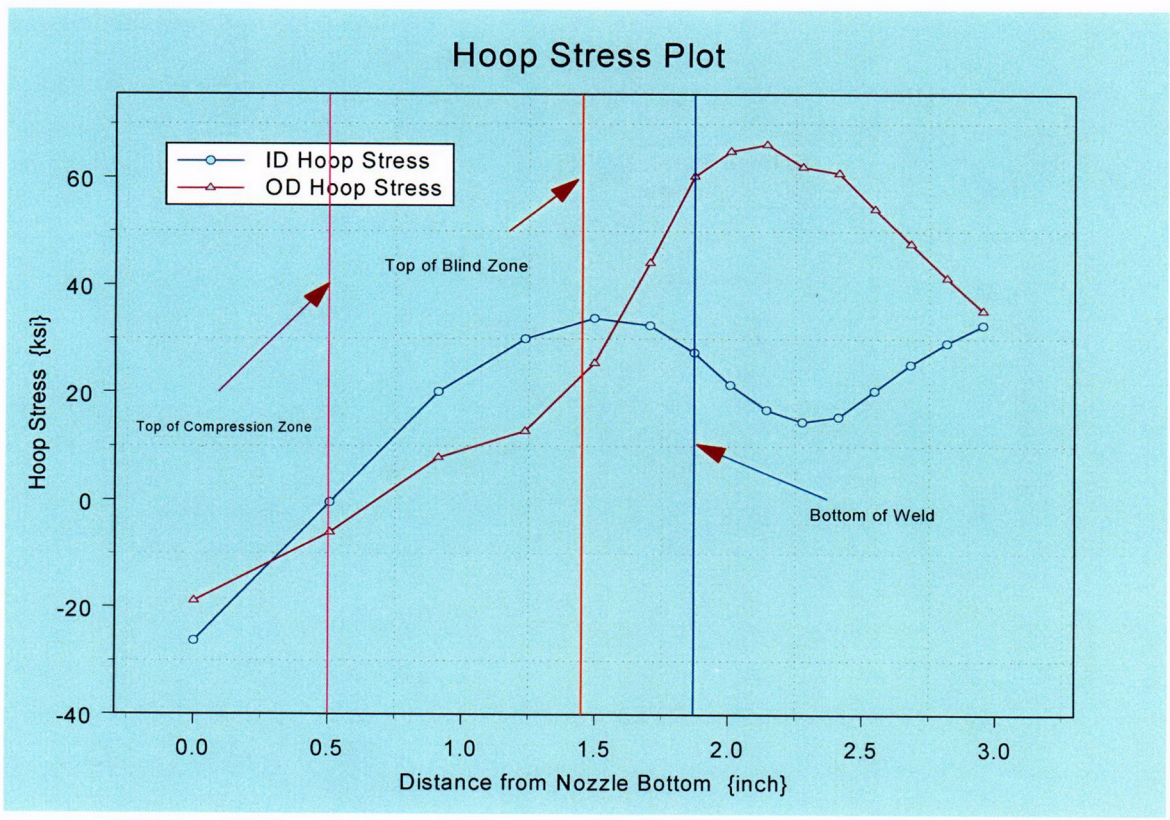


**Figure 11:** *Plot showing hoop stress distribution along tube axis for the 8.8° nozzle at 45° rotated from the downhill location. The top of compressive zone, the top of blind zone, and the bottom of the weld are shown.*

C07

| Row | Height | ID | 25% | 50% | 75% | OD |
|---|---|---|---|---|---|---|
| 30001 | 0 | -25.236 | -22.713 | -21.175 | -19.868 | -18.802 |
| 30101 | 0.53254 | -1.2673 | -2.9633 | -4.403 | -5.6895 | -6.8335 |
| 30201 | 0.95918 | 21.942 | 17.089 | 13.361 | 10.182 | 6.3275 |
| 30301 | 1.301 | 30.023 | 26.373 | 22.21 | 17.121 | 11.241 |
| 30401 | 1.5748 | 34.094 | 28.085 | 24.306 | 22.834 | 23.834 |
| 30501 | 1.7941 | 32.716 | 28.035 | 26.605 | 32.916 | 43.289 |
| 30601 | 1.9699 | 27.602 | 28.447 | 30.151 | 42.181 | 58.888 |
| 30701 | 2.1061 | 21.457 | 24.92 | 31.944 | 46.103 | 63.871 |
| 30801 | 2.2422 | 16.731 | 22.988 | 32.591 | 47.9 | 65.049 |
| 30901 | 2.3784 | 14.342 | 21.261 | 33.406 | 47.848 | 61.204 |
| 31001 | 2.5145 | 15.204 | 20.994 | 32.436 | 45.675 | 60.976 |
| 31101 | 2.6507 | 19.799 | 21.653 | 30.997 | 42.11 | 55.015 |
| 31201 | 2.7869 | 24.558 | 24.206 | 29.798 | 39.607 | 48.995 |
| 31301 | 2.923 | 28.72 | 27.503 | 32.15 | 37.459 | 42.682 |
| 31401 | 3.0592 | 32.844 | 30.245 | 35.773 | 41.844 | 36.257 |

**Table 5:** *Nodal stress for 8.8° nozzle at 67.5° rotated from the downhill location. The weld location is shown by the shaded row.*

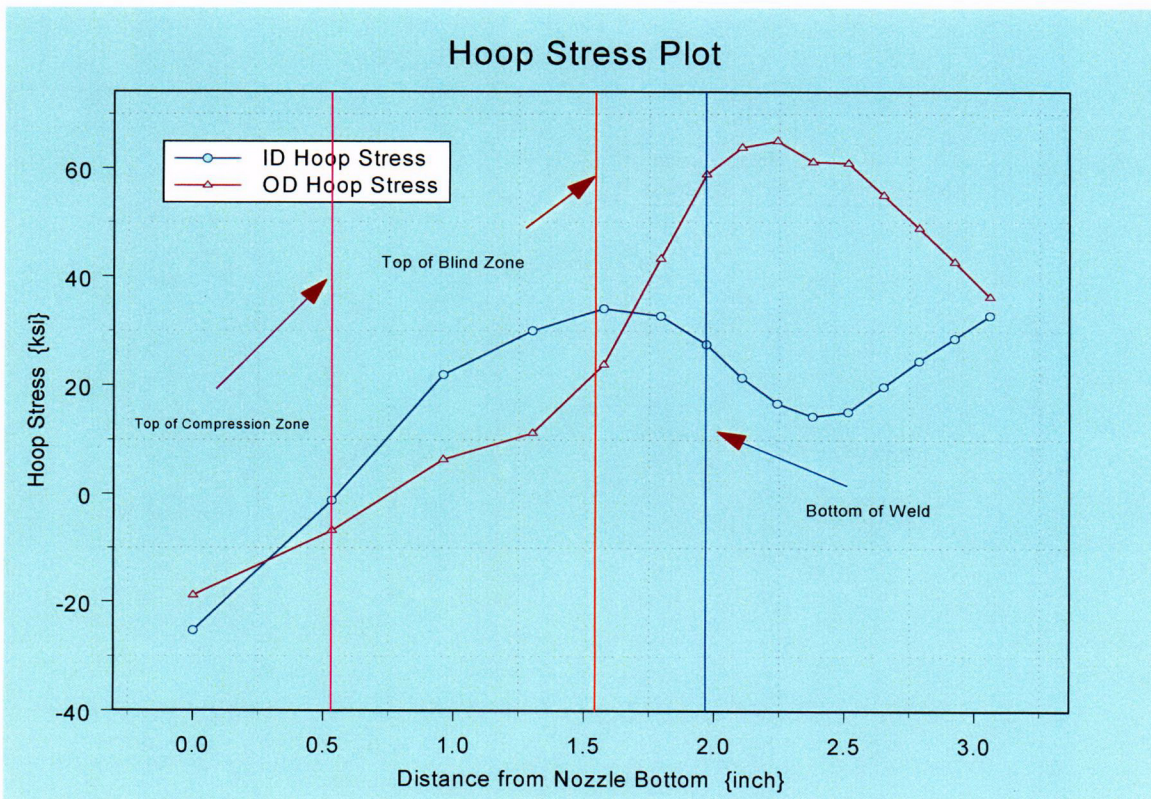


**Figure 12:** *Plot showing hoop stress distribution along tube axis for the 8.8° nozzle at 67.5° rotated from the downhill location. The top of compressive zone, the top of blind zone, and the bottom of the weld are shown.*

C08

| Row | Height | ID | 25% | 50% | 75% | OD |
|---|---|---|---|---|---|---|
| 40001 | 0.000 | -24.18 | -21.838 | -20.55 | -19.438 | -18.504 |
| 40101 | 0.564 | -1.4119 | -3.3196 | -4.9822 | -6.4762 | -7.7535 |
| 40201 | 1.016 | 22.032 | 16.773 | 12.529 | 8.7215 | 4.4282 |
| 40301 | 1.378 | 29.956 | 26.483 | 21.849 | 16.053 | 9.4283 |
| 40401 | 1.668 | 34.51 | 28.439 | 24.198 | 22.09 | 22.082 |
| 40501 | 1.900 | 33.218 | 28.069 | 26.319 | 32.416 | 42.48 |
| 40601 | 2.087 | 28.217 | 28.594 | 29.911 | 41.713 | 57.592 |
| 40701 | 2.224 | 22.006 | 25.059 | 31.606 | 45.624 | 63.118 |
| 40801 | 2.361 | 17.219 | 23.064 | 32.349 | 47.567 | 64.115 |
| 40901 | 2.499 | 14.675 | 21.28 | 33.218 | 47.796 | 60.65 |
| 41001 | 2.636 | 15.505 | 21.064 | 32.273 | 45.911 | 61.401 |
| 41101 | 2.773 | 19.832 | 21.649 | 31.008 | 42.649 | 56.171 |
| 41201 | 2.911 | 24.356 | 24.044 | 29.89 | 40.44 | 50.554 |
| 41301 | 3.048 | 28.385 | 27.206 | 32.287 | 37.721 | 43.702 |
| 41401 | 3.185 | 31.93 | 29.733 | 35.809 | 42.479 | 38.37 |

**Table 6:** *Nodal stress for 8.8° nozzle at (Mid-Plane) 90° rotated from the downhill location. The weld location is shown by the shaded row.*

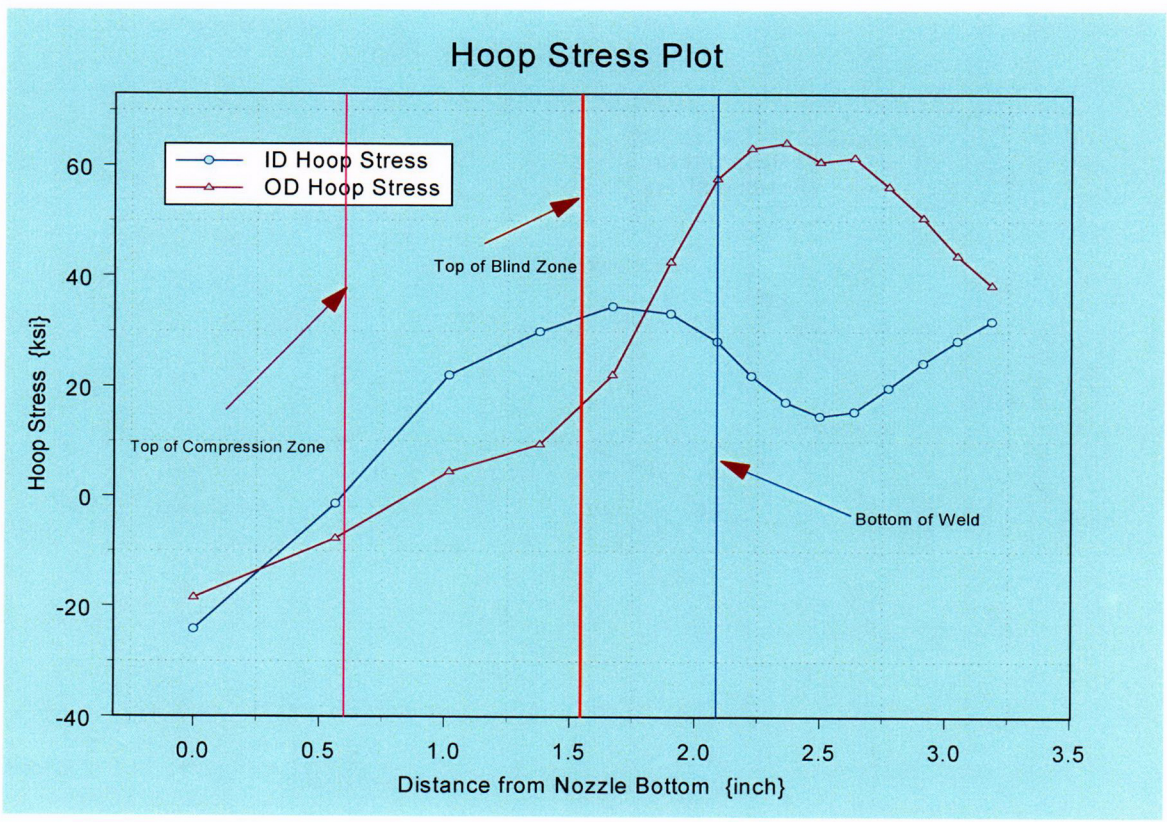


**Figure 13:** *Plot showing hoop stress distribution along tube axis for the 8.8° nozzle at (Mid-Plane) 90° rotated from the downhill location. The top of compressive zone, the top of blind zone, and the bottom of the weld are shown.*

| Row | Height | ID | 25% | 50% | 75% | OD |
|---|---|---|---|---|---|---|
| 80001 | 0.000 | -22.34 | -20.022 | -18.961 | -18.087 | -17.153 |
| 80101 | 0.645 | -0.72174 | -3.6673 | -6.8206 | -8.6957 | -10.19 |
| 80201 | 1.162 | 17.28 | 14.912 | 9.6529 | 3.7661 | -1.2205 |
| 80301 | 1.576 | 29.359 | 26.501 | 20.582 | 13.796 | 4.7531 |
| 80401 | 1.907 | 36.503 | 30.924 | 25.411 | 21.15 | 18.374 |
| 80501 | 2.173 | 36.536 | 30.331 | 27.24 | 32.606 | 41.485 |
| 80601 | 2.386 | 33.132 | 31.54 | 31.442 | 42.452 | 57.257 |
| 80701 | 2.528 | 27.116 | 28.37 | 33.434 | 47.233 | 63.826 |
| 80801 | 2.670 | 21.957 | 26.115 | 34.408 | 48.851 | 63.884 |
| 80901 | 2.813 | 18.993 | 24.124 | 35.202 | 49.904 | 62.107 |
| 81001 | 2.955 | 19.578 | 24.12 | 34.376 | 48.405 | 64.458 |
| 81101 | 3.098 | 23.12 | 24.375 | 33.301 | 45.647 | 61.604 |
| 81201 | 3.240 | 26.499 | 26.538 | 32.257 | 43.763 | 56.525 |
| 81301 | 3.382 | 29.872 | 29.202 | 35.086 | 41.634 | 49.89 |
| 81401 | 3.525 | 32.509 | 30.842 | 37.607 | 45.45 | 40.77 |

**Table 7:** *Nodal stress for 8.8° nozzle at (Uphill) 180° rotated from the downhill location. The weld location is shown by the shaded row.*

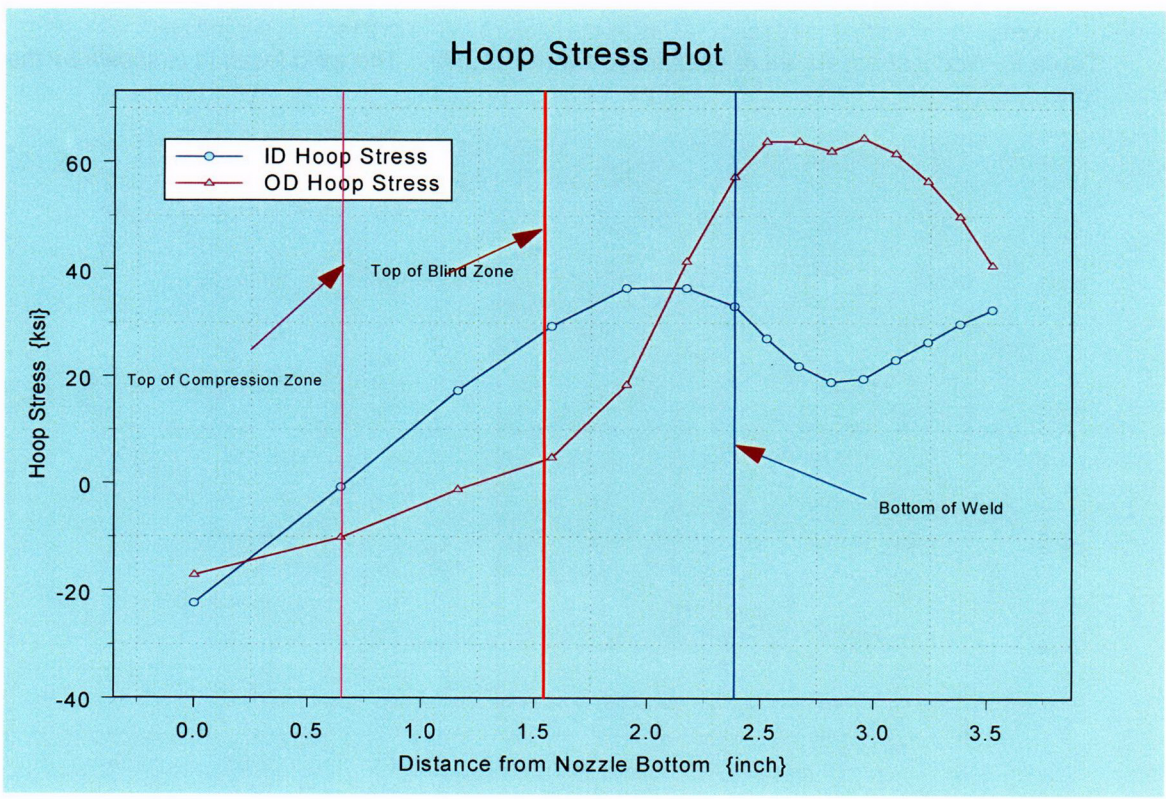


**Figure 14:** *Plot showing hoop stress distribution along tube axis for the 8.8° nozzle at (Uphill) 180° rotated from the downhill location. The top of compressive zone, the top of blind zone, and the bottom of the weld are shown.*

| Row | Height | ID | 25% | 50% | 75% | OD |
|---|---|---|---|---|---|---|
| 1 | 0.000 | -17.414 | -13.552 | -11.113 | -8.8843 | -6.6283 |
| 101 | 0.461 | -8.4943 | -6.31 | -4.924 | -3.7058 | -2.5412 |
| 201 | 0.830 | 0.088906 | 0.17947 | 0.11003 | 0.18625 | 0.2839 |
| 301 | 1.126 | 7.0251 | 6.9534 | 6.3144 | 5.2078 | 4.6462 |
| 401 | 1.363 | 8.2154 | 10.954 | 10.85 | 9.5121 | 5.6465 |
| 501 | 1.552 | 13.266 | 16.41 | 16.061 | 17.131 | 25.256 |
| 601 | 1.704 | 20.627 | 22.237 | 25.413 | 43.58 | 53.784 |
| 701 | 1.825 | 29.036 | 28.83 | 31.285 | 53.547 | 64.082 |
| 801 | 1.946 | 33.945 | 30.929 | 36.407 | 61.6 | 71.01 |
| 901 | 2.066 | 29.591 | 31.788 | 40.536 | 64.612 | 76.418 |
| 1001 | 2.187 | 23.26 | 29.738 | 41.2 | 64.193 | 79.626 |
| 1101 | 2.308 | 18.689 | 27.734 | 41.29 | 61.777 | 78.117 |
| 1201 | 2.428 | 15.391 | 26.097 | 40.668 | 58.596 | 72.784 |
| 1301 | 2.549 | 14.546 | 24.118 | 39.369 | 54.107 | 62.074 |
| 1401 | 2.670 | 16.833 | 23.402 | 37.135 | 47.479 | 45.328 |
| 1501 | 2.790 | 22.94 | 24.557 | 33.686 | 39.867 | 31.733 |
| 1601 | 2.911 | 30.347 | 28.824 | 34.637 | 35.903 | 24.215 |
| 1701 | 3.032 | 36.319 | 33.178 | 37.13 | 37.761 | 22.663 |
| 1801 | 3.152 | 40.587 | 36.14 | 41.105 | 36.249 | -4.0021 |

**Table 8:** *Nodal stress for 28.8° nozzle at downhill location. The weld location is shown by the shaded row.*

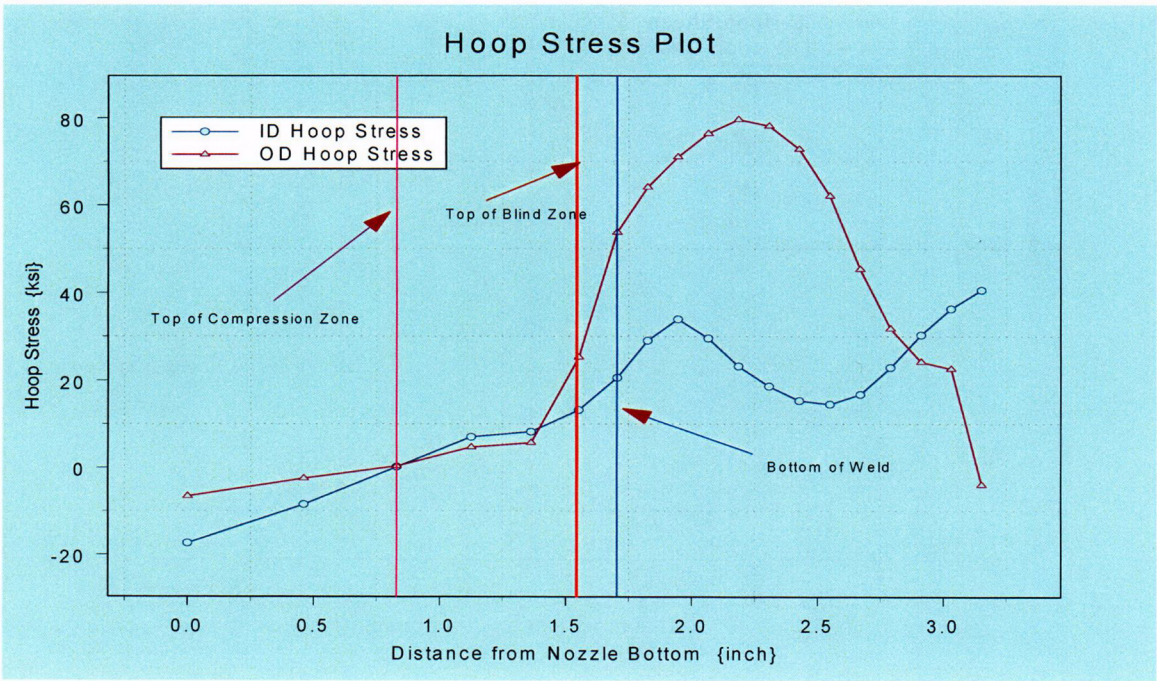


**Figure 15:** *Plot showing hoop stress distribution along tube axis for the 28.8° nozzle at downhill location. The top of compressive zone, the top of blind zone, and the bottom of the weld are shown.*

C11

| Row | Height | ID | 25% | 50% | 75% | OD |
|---|---|---|---|---|---|---|
| 10001 | 0 | -14.205 | -11.506 | -9.7904 | -8.2433 | -6.7219 |
| 10101 | 0.49517 | -6.4931 | -5.1879 | -4.4249 | -3.7959 | -3.1762 |
| 10201 | 0.89187 | 1.5545 | 1.0213 | 0.5647 | 0.25683 | -0.0759 |
| 10301 | 1.2097 | 8.4295 | 7.9804 | 7.1986 | 6.1861 | 5.292 |
| 10401 | 1.4643 | 10.247 | 12.709 | 12.22 | 11.35 | 8.3641 |
| 10501 | 1.6682 | 15.665 | 18.335 | 18.703 | 20.835 | 29.697 |
| 10601 | 1.8317 | 24.321 | 24.532 | 26.71 | 44.525 | 57.729 |
| 10701 | 1.9511 | 31.496 | 28.696 | 31.228 | 53.015 | 63.555 |
| 10801 | 2.0706 | 31.975 | 30.109 | 35.633 | 59.449 | 69.026 |
| 10901 | 2.1901 | 26.833 | 29.946 | 38.369 | 61.124 | 72.691 |
| 11001 | 2.3096 | 20.84 | 27.287 | 38.5 | 59.952 | 75.043 |
| 11101 | 2.4291 | 15.99 | 24.671 | 38.159 | 58.169 | 73.854 |
| 11201 | 2.5486 | 12.461 | 22.874 | 37.588 | 54.954 | 67.711 |
| 11301 | 2.6681 | 11.21 | 20.931 | 36.521 | 51.142 | 59.155 |
| 11401 | 2.7876 | 13.526 | 20.476 | 34.299 | 45.784 | 43.711 |
| 11501 | 2.9071 | 19.78 | 22.135 | 31.566 | 38.968 | 31.028 |
| 11601 | 3.0266 | 26.712 | 26.192 | 32.945 | 36.476 | 24.484 |
| 11701 | 3.1461 | 32.478 | 30.015 | 35.497 | 38.328 | 23.185 |
| 11801 | 3.2656 | 36.911 | 32.504 | 38.269 | 35.608 | 2.1982 |

**Table 9:** *Nodal stress for 28.8° nozzle at 22.5° rotated from the downhill location. The weld location is shown by the shaded row.*

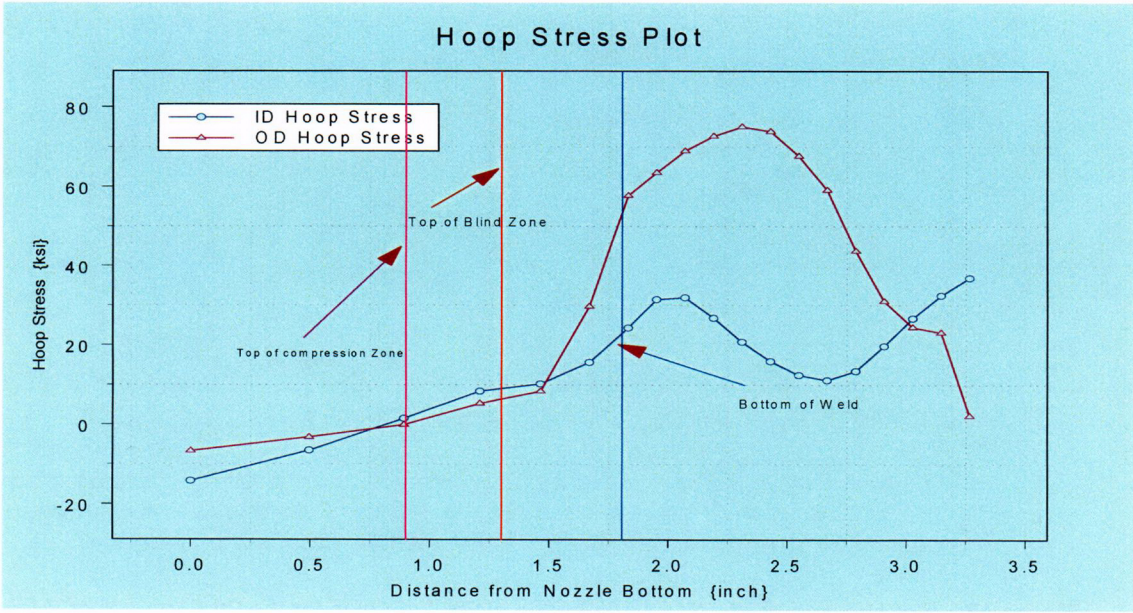


**Figure 16:** *Plot showing hoop stress distribution along tube axis for the 28.8° nozzle at 22.5° rotated from the downhill location. The top of compressive zone, the top of blind zone, and the bottom of the weld are shown.*

C12

| Row | Height | ID | 25% | 50% | 75% | OD |
|---|---|---|---|---|---|---|
| 40001 | 0.000 | 2.0791 | -0.87476 | -2.9601 | -4.82 | -6.7498 |
| 40101 | 0.811 | 0.091 | -2.3704 | -4.267 | -6.0042 | -7.5523 |
| 40201 | 1.460 | 5.2826 | 1.6859 | -0.78573 | -2.4896 | -3.4686 |
| 40301 | 1.980 | 16.881 | 12.419 | 9.564 | 6.9075 | 4.3191 |
| 40401 | 2.397 | 24.144 | 20.894 | 18.115 | 16.59 | 14.513 |
| 40501 | 2.731 | 26.962 | 22.672 | 20.686 | 24.842 | 33.523 |
| 40601 | 2.999 | 23.279 | 20.902 | 21.706 | 37.111 | 47.395 |
| 40701 | 3.113 | 17.161 | 17.101 | 20.743 | 41.091 | 51.762 |
| 40801 | 3.228 | 11.722 | 14.424 | 21.34 | 43.543 | 53.688 |
| 40901 | 3.343 | 6.0041 | 11.108 | 20.912 | 43.833 | 54.154 |
| 41001 | 3.457 | 1.439 | 8.0852 | 20.38 | 43.021 | 57.025 |
| 41101 | 3.572 | -2.1749 | 5.8905 | 19.929 | 42.405 | 56.415 |
| 41201 | 3.687 | -4.7249 | 4.8584 | 19.994 | 40.425 | 58.85 |
| 41301 | 3.801 | -4.9201 | 4.8793 | 20.34 | 38.451 | 57.617 |
| 41401 | 3.916 | -2.8845 | 6.4727 | 20.545 | 37.523 | 49.152 |
| 41501 | 4.031 | 0.86049 | 8.0075 | 21.386 | 36.18 | 40.228 |
| 41601 | 4.145 | 5.584 | 11.001 | 22.915 | 36.59 | 35.152 |
| 41701 | 4.260 | 9.8086 | 14.62 | 25.477 | 36.977 | 32.699 |
| 41801 | 4.375 | 17.392 | 18.195 | 28.176 | 40.112 | 19.759 |

**Table 10:** *Nodal stress for 28.8° nozzle at (Mid-Plane) 90° rotated from the downhill location. The weld location is shown by the shaded row.*

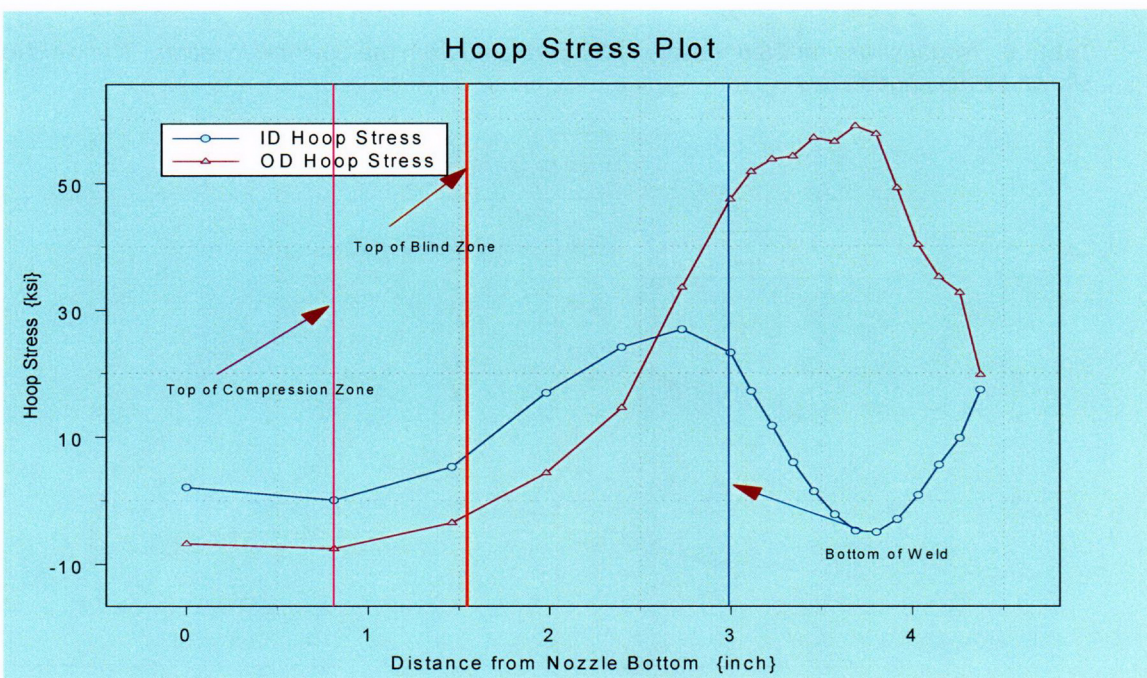


**Figure 17:** *Plot showing hoop stress distribution along tube axis for the 28.8° nozzle at (Mid-Plane) 90° rotated from the downhill location. The top of compressive zone, the top of blind zone, and the bottom of the weld are shown.*

C13

| Row | Height | ID | 25% | 50% | 75% | OD |
|---|---|---|---|---|---|---|
| 80001 | 0.000 | -9.0335 | -5.8552 | -4.2456 | -2.6894 | -1.0312 |
| 80101 | 1.154 | -6.761 | -6.7389 | -7.2366 | -7.6623 | -7.8035 |
| 80201 | 2.078 | 7.9654 | 1.7419 | -6.2304 | -11.848 | -16.387 |
| 80301 | 2.819 | 23.851 | 21.763 | 8.5552 | -6.3899 | -17.647 |
| 80401 | 3.412 | 43.99 | 38.072 | 29.826 | 13.47 | -1.6316 |
| 80501 | 3.888 | 47.954 | 41.753 | 35.453 | 33.324 | 35.846 |
| 80601 | 4.268 | 43.756 | 39.214 | 38.4 | 53.023 | 57.543 |
| 80701 | 4.377 | 40.773 | 36.237 | 41.27 | 61.453 | 62.189 |
| 80801 | 4.486 | 39.277 | 35.327 | 44.863 | 64.204 | 63.895 |
| 80901 | 4.595 | 36.022 | 35.389 | 46.842 | 64.323 | 62.934 |
| 81001 | 4.704 | 33.54 | 36.173 | 48.06 | 64.483 | 66.03 |
| 81101 | 4.813 | 32.631 | 36.616 | 47.779 | 67.612 | 70.356 |
| 81201 | 4.922 | 32.794 | 36.656 | 47.356 | 66.386 | 72.973 |
| 81301 | 5.031 | 33.889 | 36.612 | 47.548 | 65.375 | 77.806 |
| 81401 | 5.140 | 35.222 | 36.179 | 47.538 | 65.411 | 75.322 |
| 81501 | 5.249 | 36.353 | 35.865 | 47.964 | 64.448 | 70.447 |
| 81601 | 5.358 | 36.426 | 36.986 | 48.341 | 62.979 | 62.511 |
| 81701 | 5.467 | 37.233 | 38.52 | 49.064 | 63.153 | 61.112 |
| 81801 | 5.575 | 40.874 | 39.218 | 48.17 | 62.039 | 57.291 |

**Table 11:** *Nodal stress for 28.8° nozzle at (Uphill) 180° rotated from the downhill location. The weld location is shown by the shaded row.*

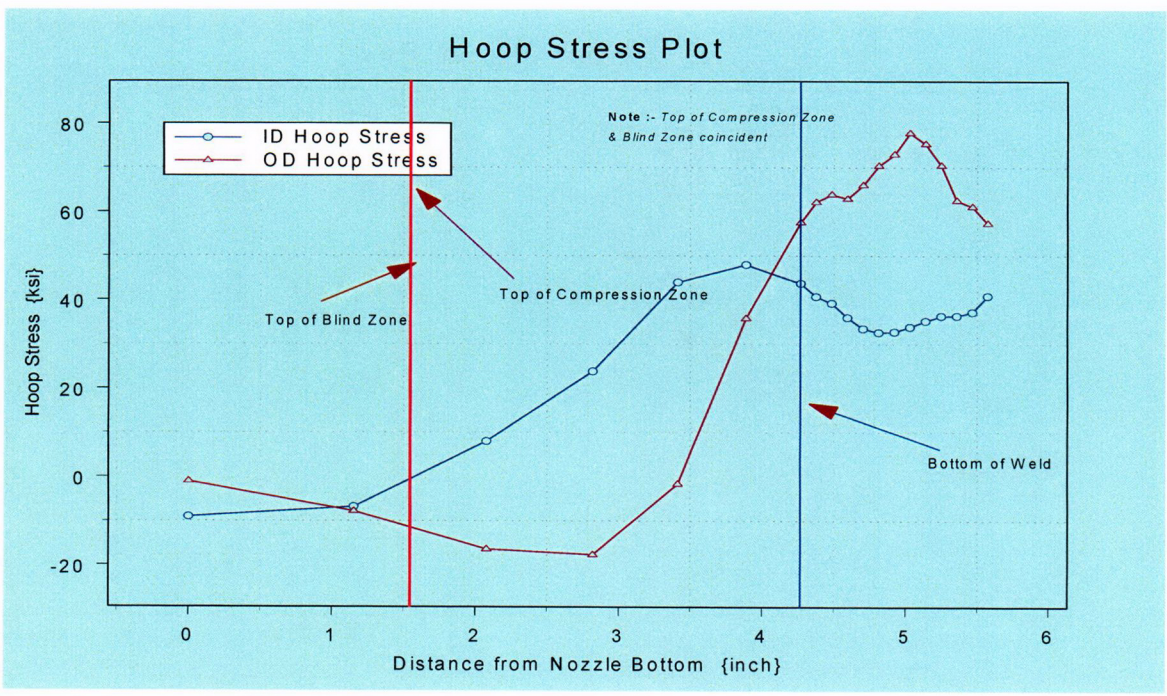


**Figure 18:** *Plot showing hoop stress distribution along tube axis for the 28.8° nozzle at (Uphill) 180° rotated from the downhill location. The top of compressive zone, the top of blind zone, and the bottom of the weld are shown.*

C14